

## Dynamical effects of momentum dependence of the nuclear mean field in medium energy heavy ion collisions

V. Greco, A. Guarnera, M. Colonna, and M. Di Toro  
*Laboratorio Nazionale del Sud, Via S. Sofia 44, I-95123 Catania, Italy*  
*and University of Catania, I-95100 Catania, Italy*  
 (Received 20 July 1998)

We suggest several ways to study the dynamical effects of the momentum dependence of the nuclear mean field in medium energy heavy ion collisions, from incomplete fusion to multifragmentation events. We present dynamical simulations based on a new transport code with a quite general form of mean field nonlocality and we compare with local effective forces giving the same equilibrium properties. We clearly see sizable effects on the onset of instabilities, on rates and angular distributions of preequilibrium particle emission, and on rapidity distributions of vaporization events for central collisions. [S0556-2813(99)03802-9]

PACS number(s): 24.10.-i, 25.70.Pq

### I. INTRODUCTION

It is well known that the presence of correlations in a nuclear system necessarily leads to a momentum dependence of the self-consistent mean field [1,2]. Experimentally it is well established that the real part of the optical potential is strongly momentum dependent [3]. Microscopically the most trivial evidence of this property comes from the intrinsic nonlocality of the Hartree-Fock potential due to the Pauli correlation. Indeed all effective forces used for microscopic calculations of nuclear structure contain some momentum dependent terms, in the simplest form as an effective mass. It is however also well known that momentum independent and momentum dependent potentials with similar saturation properties, binding energy density, and compressibility give similar equilibrium parameters for excited nuclear matter. Therefore a thorough study of momentum dependence can be only based on observables associated with nonequilibrium dynamics, i.e., collective modes and reaction mechanisms. Many theoretical analyses have appeared on the study of momentum dependence effects on collective flow and balance energy, i.e., on the transition from mean field to hydrodynamical regimes in the reaction mechanisms for intermediate and high energy heavy ion collisions [4–6]. The motivation was that with local forces the data could be reproduced only using an equation of state with a quite unrealistic high stiffness.

However, the most difficult problem has been the fact that another quite essential nonequilibrium parameter, the in-medium nucleon-nucleon ( $NN$ ) cross section, can easily mock up the dynamical effects of a momentum dependence, larger repulsion, and fewer two-body collisions.

In this paper we will try to show that it is possible to extract independent information on these two important nonequilibrium properties, the  $NN$  cross section and the velocity dependence of the mean field. Moreover, we will see that momentum dependence leads to observable effects also on low energy reaction mechanisms.

After a short discussion about nonlocality effects on the collective nuclear response we will focus our attention on two quite different physical scenarios for reaction mecha-

nisms in heavy ion collisions: (i) preequilibrium emission in incomplete fusion events at relatively low energies and (ii) vaporization events in central collisions at intermediate energies. We will show that spectra and angular distributions of fast emitted particles [case (i)] and rapidity distributions [case (ii)] are particularly sensitive to the momentum dependence of the mean field and not much affected by  $\sigma_{NN}$  variations.

We will use the Gale–Bertsch–Das Gupta (GBD) form of the mean field nonlocality, constructed on a Skyrme-type effective interaction [4]. We remark that in a quite large dynamical range  $\rho/\rho_0 \leq 1.5$  and momenta  $0 \leq k \leq 4 \text{ fm}^{-1}$ , the results are quite similar to other nonlocal forces of the Gogny type [7,8]. So we are confident that the effects discussed here are not related to the particular parametrization of the velocity dependence used.

In Sec. II we introduce the new transport equation code for simulations with momentum dependent fields. In Sec. III we analyze incomplete fusion reactions discussing some effects on density oscillations and on preequilibrium particle emission. In Sec. IV we show some results for vaporization events and finally some conclusions are drawn in Sec. V.

### II. NUCLEAR DYNAMICS WITH MOMENTUM DEPENDENT FIELDS

We have extended the well-established Boltzmann-Nordheim-Vlasov transport approach [2,9–13] to a momentum dependent mean field. We have considered the quite general GBD form [4,8] of momentum dependence in a Skyrme-like effective mean field:

$$U(\rho, \mathbf{p}) = A \left( \frac{\rho}{\rho_0} \right) + B \left( \frac{\rho}{\rho_0} \right)^{7/6} + \frac{C}{\rho_0} \int d^3 \mathbf{p}' \frac{f(\mathbf{r}, \mathbf{p}')}{1 + \left( \frac{\mathbf{p}' - \langle \mathbf{p}' \rangle}{\Lambda} \right)^2} + C \frac{\rho}{\rho_0} \frac{1}{1 + \left( \frac{\mathbf{p} - \langle \mathbf{p} \rangle}{\Lambda} \right)^2}, \quad (2.1)$$

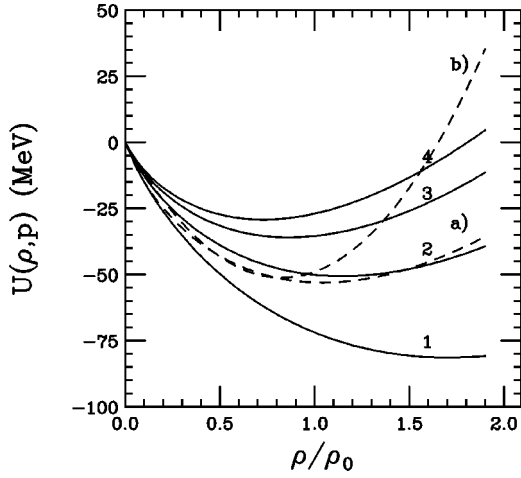


FIG. 1. Density dependence of the GBD mean field (solid lines). The labels give  $p$  values in  $\text{fm}^{-1}$ . Dashed lines show the local mean field for (a) soft choice and (b) stiff choice.

where  $A = -144.9$  MeV,  $B = 203.3$  MeV,  $C = -75$  MeV, and  $\Lambda = 1.5p_F(0)$ ,  $p_F(0)$  being the Fermi momentum at saturation density  $\rho_0$ . The corresponding potential energy density gives nuclear matter (NM) saturation properties  $E/A = -16$  MeV,  $\rho_0 = 0.163$   $\text{fm}^{-3}$ , and a compressibility modulus  $K = 215$  MeV, i.e., a *soft* equation of state (EOS) [4]. The parameters are chosen also in order to have

$$\left. \frac{d}{d\rho} U(\rho_0, p) \right|_{p=p_F} = 0.43 \frac{p_F}{m},$$

and so an effective mass, at  $\rho_0$ ,  $m^* = 0.7m$ . Here  $\langle \mathbf{p}(\mathbf{r}) \rangle$  represents the collective momentum in a space cell around  $(\mathbf{r})$ .

In cold nuclear matter,  $\langle \mathbf{p} \rangle = 0$  and  $f(\mathbf{r}, \mathbf{p}) = 4/h^3 \Theta(\mathbf{p} - \mathbf{p}_F)$ ; so we have a field

$$U(\rho, \mathbf{p}) = A \left( \frac{\rho}{\rho_0} \right) + B \left( \frac{\rho}{\rho_0} \right)^{7/6} + C \frac{\rho}{\rho_0} \frac{1}{1 + \left( \frac{\mathbf{p}}{\Lambda} \right)^2} + \frac{16C\pi}{\rho_0 h^3} \Lambda^3 \{ p_F(\rho)/\Lambda - \arctan[p_F(\rho)/\Lambda] \}. \quad (2.2)$$

Since  $C < 0$ , we see that for a fixed density we have more repulsion for particles with higher momenta. In the following we will compare results in collision dynamics with two momentum independent mean field parametrizations

$$U(\rho) = A \left( \frac{\rho}{\rho_0} \right) + B \left( \frac{\rho}{\rho_0} \right)^\sigma, \quad (2.3)$$

with parameters fixed in order to have the same cold NM binding energy and saturation density, but two different compressibility values:

$$(a) K = 200 \text{ MeV (soft local)}, \quad A = -356 \text{ MeV},$$

$$B = 303 \text{ MeV}, \quad \sigma = 7/6,$$

$$(b) K = 380 \text{ MeV (stiff local)}, \quad A = -124 \text{ MeV},$$

$$B = 70.5 \text{ MeV}, \quad \sigma = 2.$$

In Fig. 1 we compare the density behavior of the momentum dependent mean field, Eq. (2.2), for different values of  $p$  in  $\text{fm}^{-1}$ , with the two local parametrizations.

Since in the interacting region of a heavy ion collision  $(\mathbf{p} - \langle \mathbf{p} \rangle)$  can reach quite high values, we expect to see large dynamical effects [8]. In this paper we show that some selected observables are very sensitive to that also at low energies.

We have worked out a new dynamical code based on the solution of the Vlasov transport equation for test particles in phase space with a two-body collision term of the Boltzmann-Nordheim type [1,9–14]. The potential energy density corresponding to the mean field, Eq. (2.1), gives the following Hamiltonian for the test particle propagation:

$$H = \sum_{i=1}^{N \cdot A} \frac{p_i^2}{2m} + \sum_{\text{cells}} (dv)_{\text{cells}} \int d^3 \mathbf{p} \rho \left\{ \left[ \frac{A}{2} \left( \frac{\rho}{\rho_0} \right) + \frac{B}{\sigma+1} \left( \frac{\rho}{\rho_0} \right)^\sigma \right] \delta(\mathbf{p}) + \frac{C}{\rho_0} \frac{f(\mathbf{r}, \mathbf{p})}{1 + \left( \frac{\mathbf{p} - \langle \mathbf{p} \rangle}{\Lambda} \right)^2} \right\} = T + V, \quad (2.4)$$

where  $N$  denotes the number of test particles per nucleon. In this way we ensure an exact energy conservation in the mean field dynamical evolution [13]. The lattice structure has been used to implement the numerical code TWINGO [14] (in order to reduce the computing time for the solution of a Vlasov equation with local fields). The Coulomb interaction is accounted for in a self-consistent way just computing the Coulomb field in each cell through the inversion of the Poisson equation from the local proton density.

We perform a Monte Carlo simulation of the collision integral [12] using an isotropic and energy-isospin averaged  $NN$  cross section  $\sigma_{NN} = 41$  mb. The effects of different cross section parametrizations will be discussed in Sec. IV.

A further important modification of the kinetic code comes from energy conservation in the collision integral since now the two-body kinetic energy conservation condition is not enough because the potential energy is also varying with the new final momenta. A simple and effective way to overcome this difficulty has been to introduce a ‘‘collective’’ shift of the final momenta of the colliding test particles:

$$\mathbf{p}_{\text{new}} = \mathbf{p}_{\text{old}} + \beta \langle \mathbf{p} \rangle, \quad (2.5)$$

where  $\langle \mathbf{p} \rangle$  is the average momentum in the cell where the collision takes place. The parameter  $\beta$  is fixed from total energy conservation at each time step. This redistribution of test particle momenta has the nice feature of keeping unchanged the quantity  $(\mathbf{p} - \langle \mathbf{p} \rangle)$  and therefore the potential energy in each cell. Various stringent tests on stability in the time evolution of an isolated nucleus and on energy conservation in a collision have been performed. Moreover, it is possible to show that the local collective shift, Eq. (2.5),

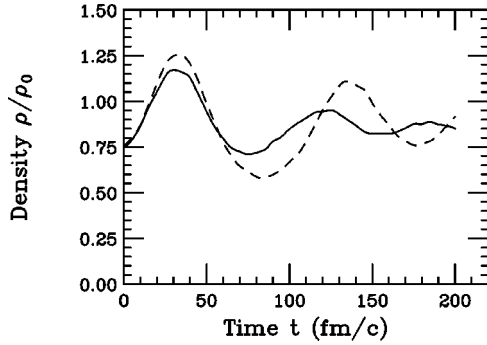


FIG. 2. Density oscillations in a sphere of radius 4 fm around the c.m. in the collision Kr+Al at 34 MeV/nucleon,  $b=1$  fm. Dashed line, soft-local EOS; solid line, GBD.

ensures momentum conservation. This is exact for the linear momentum and represents a very good approximation for the angular momentum, based on the use of the mean space coordinate of the cell as the position where the test-particle collision takes place. As a result of the large number of cells on average, we have a compensation of small deviations and the total angular momentum is very well conserved. This also has been checked numerically.

With this new code we are now ready to analyze dynamical simulations of various heavy ion collisions at medium energies.

### III. INCOMPLETE FUSION EVENTS: DENSITY OSCILLATIONS AND PREEQUILIBRIUM EMISSION

We have studied first the reactions  $^{84}\text{Kr} + ^{27}\text{Al}$  at 34.4 MeV/nucleon and  $^{139}\text{La} + ^{27}\text{Al}$  at 55 MeV/nucleon, previously analyzed in the fragmentation channel with a local mean field code using a soft EOS parametrization [15,16], and where data are also available for different reaction mechanisms [17,16].

For the impact parameter  $b=1$  fm, we have mostly incomplete fusion events. Here we will stress the differences in the dynamical evolution due to the momentum dependence of the mean field.

Incomplete fusion events are characterized by monopole oscillations of the bulk density up to the formation of an equilibrated hot residue after some fast particle emission. In Fig. 2 we report the time evolution of the mean density in a sphere of 4 fm radius around the center of mass (c.m.) in the Kr+Al case, in the *soft-local* [Eq. (2.3)] and GBD mean field cases. Although the compressibility is nearly the same, we clearly see different amplitudes and frequencies of the oscillations.

Momentum dependence is inducing more repulsion and therefore a reduction of the density variations but also an increase of the monopole frequency due to the presence of effective masses. These effects are difficult to check experimentally. There are however other observables, related to preequilibrium emission, also very sensitive to nonlocality and easier to measure.

In Fig. 3(a) we present the time evolution of the number of nucleons emitted during the same collision. We clearly see a larger emission for the GBD case which takes place essentially during the first 100 fm/c. This initial period cor-

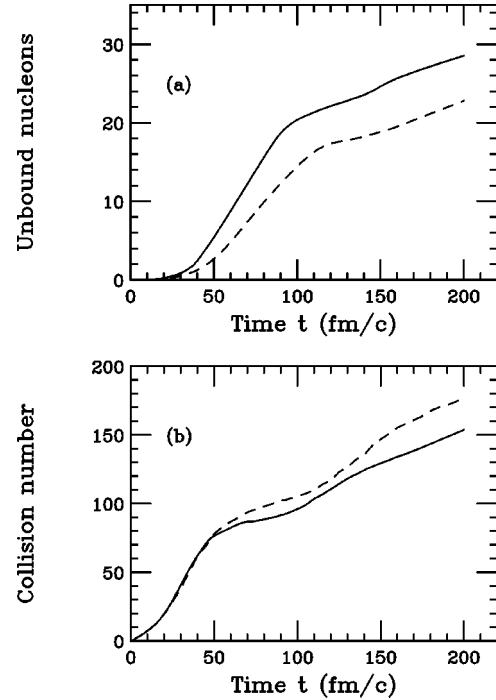


FIG. 3. (a) Time evolution of nucleon emission rate in the collision Kr+Al at 34 MeV/nucleon,  $b=1$  fm. Dashed line, soft-local EOS; solid line, GBD. (b) Time evolution of the nucleon-nucleon collisions in the same simulation. Dashed line, soft-local EOS; solid line, GBD.

responds to the preequilibrium stage of the reaction, as we can recognize from the slope variation in Fig. 3(a) and from other checks on the particle mean energy and on the sphericity of the momentum distributions [15]. A quite different hot residue is formed in the case of the momentum dependence, with a smaller number of particles and lower excitation energy [18]. As we can see from Fig. 3(a) we have a more than 15% difference in the prediction of the residue mass, a good observable that can be checked experimentally.

Which is the physical mechanism of that larger preequilibrium emission in the case of the momentum dependent mean field?

In Fig. 3(b) we report the time evolution of the number of nucleon-nucleon collisions. We expect two competing effects on the frequency of two-body collisions from momentum dependence since while the mean free path is increasing due to the smaller density variation the mean particle velocity is also increasing due to the effective mass. From Fig. 3(b) we see that after about 50 fm/c, i.e., still in the preequilibrium stage, the number of collisions becomes smaller in the GBD case, as one would expect from the repulsion effects already noticed from Fig. 2. We have in Fig. 5(b) the same behavior for the La+Al case.

The larger number of emitted nucleons is then due to a *one-body* mechanism, i.e., a smaller attraction of the momentum dependent mean field which is now less able to keep higher momentum nucleons in the interacting region. We expect then to have a dominant preequilibrium emission of *Fermi jet* type, strongly focused in the forward or backward direction.

The same analysis has been performed for the La+Al reaction at higher energy, 55 MeV/nucleon, comparing also

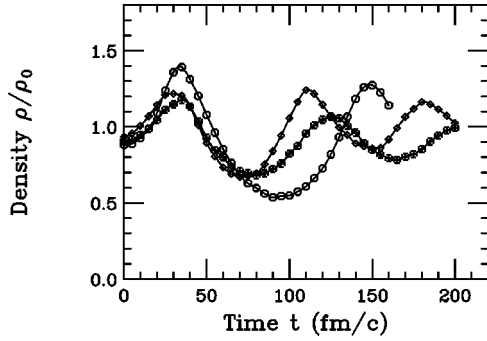


FIG. 4. Density oscillations in a sphere of radius 4 fm around the c.m. in the collision La+Al at 55 MeV/nucleon,  $b=1$  fm. Circles, soft-local EOS; diamonds, stiff-local EOS; Greek crosses, GBD.

with the results of simulations with an effective force of the *stiff-local* type. Figure 4 is the correspondent of Fig. 2, i.e., density oscillations around the center of mass. With respect to the soft-local potential we see a larger monopole frequency due to the effective mass, since the compressibility is roughly the same. Moreover, in the soft-local case we have oscillations of larger amplitude, with the possibility of exploring highly dilute regions of nuclear matter, where we can expect spinodal instabilities to show up. We can then predict noticeable differences in the reaction mechanism for central collisions in this energy range. We remark that the amplitude of the oscillations is larger also in the stiff-local case, although here the compressibility is about twice the value given by the momentum dependent mean field. This effect has been already observed also for other nonlocal fields [6,19].

Figure 5 confirms the results already stressed for the lower energy case, i.e., a larger preequilibrium nucleon emission correlated to a smaller number of two-body collisions, for the “momentum dependent” simulation. As we can see from Fig. 5(a), at higher energy the difference in the rate of prompt emitted particles can reach almost 30%, with very noticeable effects on properties of the heavy residue left. We remark in Fig. 5(b) the variation in the number of collisions just following the density oscillations on Fig. 4. The important point to stress is that in the case of local forces the stiffness of the EOS is not much influencing the preequilibrium emission. This means that the fast particle emission and the related features of the remaining heavy residue will be very sensitive to the nonlocality of the effective mean field.

We do not have a direct experimental measurement of the hot residue properties for the two studied systems. However, if we look at the analysis of the final charge production cross sections performed in Ref. [15] (see Figs. 9 and 10), with a local mean field, we realize that a residue with lower average mass and excitation energy will lead to a better agreement with data after the evaporation cascade.

The mechanism of “Fermi jets” for that enhanced nucleon emission has been confirmed from the analysis of the relative angular distribution; see Fig. 6. The backward increase in the c.m. reference system comes from the inverse kinematics of the reaction which implies that the most energetic nucleons that are not stopped by the mean field will come from the target. Exactly on this part of the fast emitted particles we see the large difference between the predictions

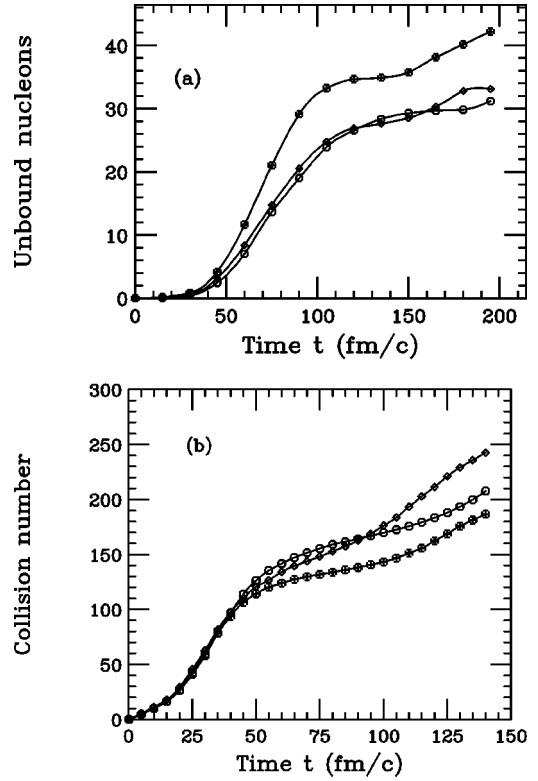


FIG. 5. (a) Time evolution of nucleon emission rate in the collision La+Al at 55 MeV/nucleon,  $b=1$  fm. Circles, soft-local EOS; diamonds, stiff-local EOS; Greek crosses, GBD. (b) Time evolution of the nucleon-nucleon collisions in the same simulation, symbols like before.

of the momentum dependent mean field and the local potentials, almost independently of their compressibility modulus. In conclusion the anisotropy of the preequilibrium particle emission seems to be another observable very sensitive to nonlocal terms. Of course in the laboratory system the effect on Fermi jets would be easier to detect in direct kinematics experiments, since these nucleons crossing the interaction zone at forward angles will move with roughly the beam velocity, and so well above the detection threshold. This is the reason why we do not have good data on angular distributions to compare with for the two studied reactions, both in inverse kinematics.

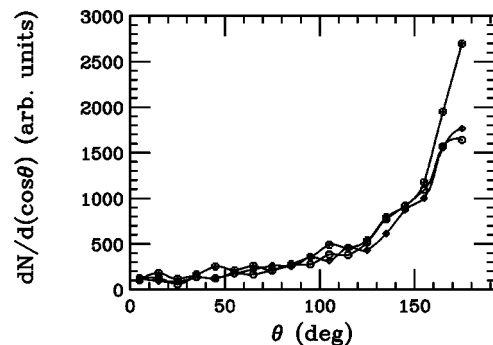


FIG. 6. Center-of-mass angular distribution of fast emitted nucleons (before  $t=100$  fm/c) in the collision La+Al at 55 MeV/nucleon,  $b=1$  fm. Circles, soft-local EOS; diamonds, stiff-local EOS; Greek crosses, GBD.

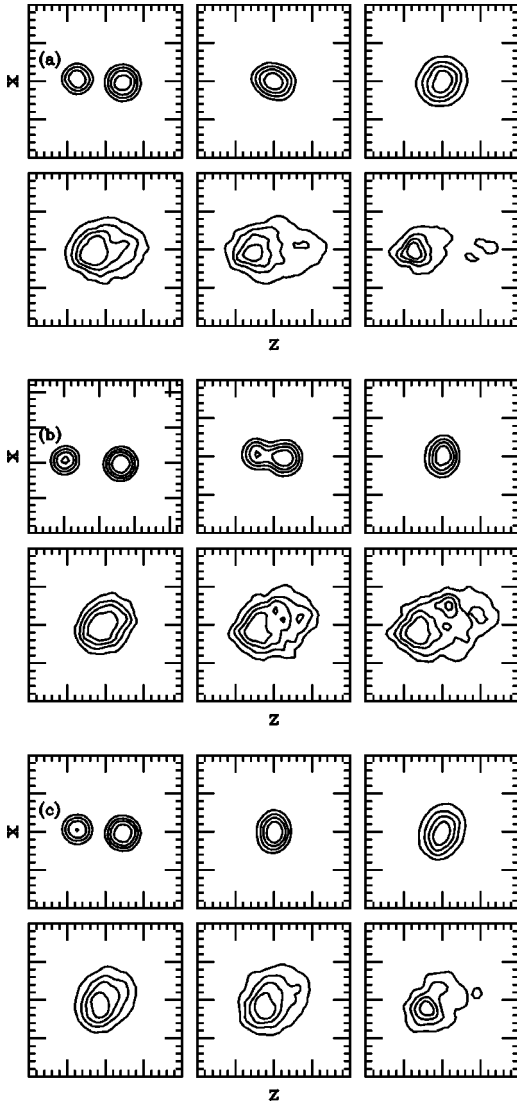


FIG. 7. Time evolution of density distributions on the reaction plane ( $z$  is along the beam axis) for the reaction Ar+Ni at 95 MeV/nucleon and  $b=1$  fm: (a) GBD mean field; (b) soft-local EOS; (c) stiff local EOS.

#### IV. VAPORIZATION EVENTS: RAPIDITY DISTRIBUTIONS

In the previous section we have seen two main effects on collision dynamics coming from the momentum dependence of the mean field: (i) a larger repulsion for high momentum particles and (ii) an overall reduction in the number of two-body collisions. Both effects are leading to a smaller *stopping power* in the interacting region of heavy ion collisions.

At larger energies we expect to see clear transparency signatures. We have studied central heavy ion collisions around 100 MeV/nucleon of beam energy, where we expect to have a relevant fraction of vaporization events, i.e., production of light fragments (charge  $Z < 3$ ) from a fast expanding source (fireball explosion) [20]. A very accurate selection of the vaporization events and the relative fragment rapidity distribution has been recently discussed by the INDRA Collaboration [21]. A large transparency would manifest through a wide rapidity distribution of the produced fragments, i.e., with an extended source on the parallel velocity axis.

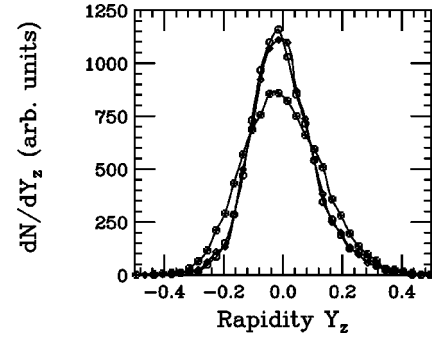


FIG. 8. Rapidity distribution of escaped nucleons obtained in the collision Ar+Ni at 95 MeV/nucleon,  $b=1$  fm. Circles, soft-local EOS; diamonds, stiff-local EOS; Greek crosses, GBD.

We have studied one of the systems of Ref. [21], the reaction  $^{36}\text{Ar} + ^{58}\text{Ni}$  at 95 MeV/nucleon and impact parameter  $b=1$  fm. Different choices of the mean field give a quite different dynamical evolution of the collision, as shown in Figs. 7(a), 7(b), and 7(c). While the compression phase is quite similar the expansion and the related fragment emission are clearly different. In particular we notice a more elongated distribution, along the beam axis, of the expanding source in the momentum dependent case with small residues left by a transparency mechanism.

At around 150 fm/c almost 80% of the nuclear matter is “vaporized,” i.e., emitted as light fragments. However, the rapidity distribution  $dN/dY_z$ , the number of nucleons vs  $Y_z \equiv \tanh^{-1}(v_{\parallel}/c)$ , is quite sensitive to the momentum dependence as shown in Fig. 8 (we choose  $Y_z=0$  for the c.m.). We clearly see less stopping power in the momentum dependent simulation, i.e., fewer nucleons emitted at zero rapidity and more at  $|Y_z| \geq 0.2$ .

The effect is present also at impact parameter  $b=3$  fm, which means no negligible cross section. We have used the GBD  $b=3$  fm rapidity distribution for a comparison with the data of Ref. [21]; see Fig. 9 (the two curves are normalized

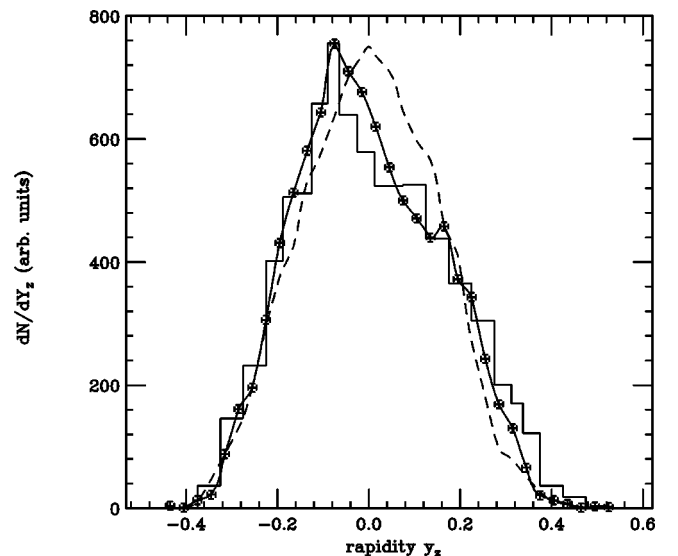


FIG. 9. Same as Fig. 9,  $b=3$  fm results (solid+Greek crosses, GBD, dashed line, stiff local EOS) vs experimental data from Ref. [21] (histogram). The curves are normalized at the peak value.

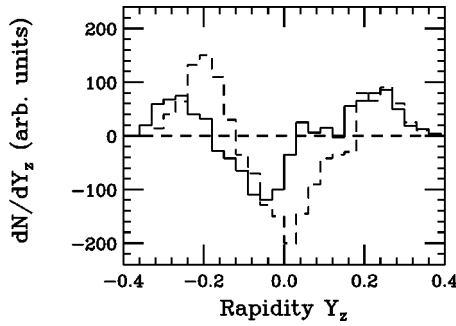


FIG. 10. Difference between GBD and soft-local rapidity distributions of nucleons emitted in the collision Ar+Ni at 95 MeV/nucleon:  $b=1$  fm, solid curve;  $b=3$  fm, dashed curve.

to the peak value). The behavior is quite similar. A local-stiff mean field (dashed line) would give a distribution too much peaked around  $Y_z=0$ . The same would happen with local-soft forces. In Fig. 10 we report the difference between the rapidity distribution obtained with GBD and the one from a local-soft mean field for  $b=1$  fm (solid line) and  $b=3$  fm (dashed line). In conclusion momentum dependence seems to be essential in order to reproduce the experimental trend.

The transparency effect will certainly show up also in the angular distributions of emitted particles. This is shown in Figs. 11(a) and 11(b). The point to stress here is that the same forward peaked anisotropy is present in the nonlocal case even when increasing up to 40% the nucleon-nucleon cross section used to simulate the collision integral [Fig. 11(b)].

This seems to be a good indication of the fact that from measurements of rapidity and angular distributions of fragments in vaporization events we can get direct information on mean field properties and related nuclear EOS, almost independently of the used *in-medium* nucleon-nucleon cross sections. As remarked in the Introduction this analysis is not unique in collective flow studies.

### V. CONCLUSIONS AND PERSPECTIVES

We have shown that the momentum dependence of the nuclear mean field has very important and observable effects on the dynamics of heavy ion collisions *also at relatively low beam energies*. Performing reaction simulations with a new computer code based on a self-consistent transport approach with a nonlocal mean field we have seen that incomplete fusion and vaporization processes are strongly affected by the momentum dependence. We remark that previous studies on the dynamical effects of nonlocality considered only transverse momenta (collective flows) at higher energies. In incomplete fusion processes we predict a larger preequilibrium nucleon emission, mostly of Fermi jet type, which can be detected as (1) a strong anisotropy in the angular distri-

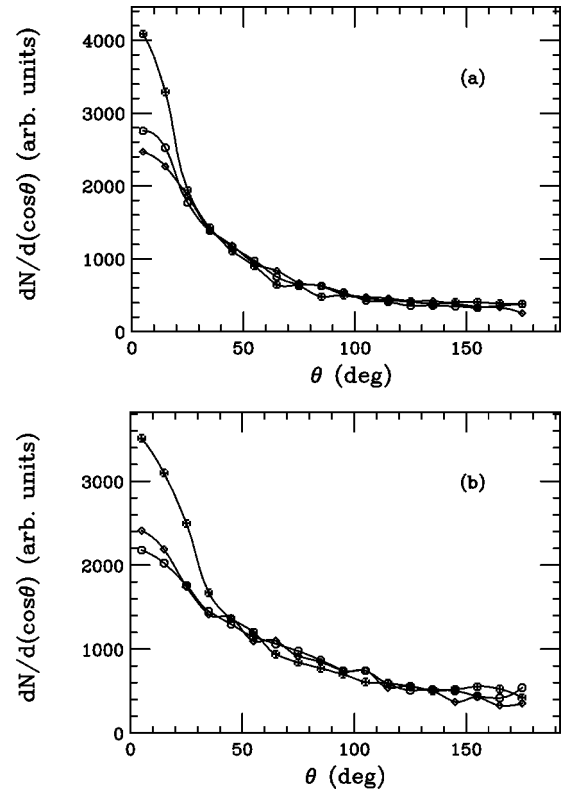


FIG. 11. Angular distribution of escaped nucleons in the collision Ar+Ni at 95 MeV/nucleon,  $b=1$  fm. Circles, soft-local EOS; diamonds, stiff-local EOS; Greek crosses, GBD. (a)  $\sigma_{\text{free}}=41$  mb nucleon-nucleon cross section; (b)  $\sigma=1.4\sigma_{\text{free}}$ .

bution, largely focused in the forward or backward direction with respect to the beam axis; (2) a targetlike (or projectile-like) mean velocity; and (3) quite reduced mass and excitation energy for the formed equilibrated heavy residue.

In fragmentation reactions for central collisions at around 100 MeV/nucleon (vaporization events), we expect a larger transparency, which seems indeed in agreement with recent INDRA data. The interesting new feature of our results relies in the fact that the effect is almost not dependent on the used *in-medium* nucleon-nucleon cross section. So it seems that from analyses of fragment rapidity and angular distributions we can overcome the problem of competing contributions from the *NN* cross section and the mean field faced in collective flow studies.

Finally, a last comment to put future work in perspective. We have clearly seen that the ‘‘dynamical’’ repulsion caused by momentum dependence leads to a net overall reduction of the number of direct nucleon-nucleon collisions. We expect a clear effect on energetic particle production. In particular the hard photon rate, well explained as a first chance incoherent proton-neutron bremsstrahlung yield in local field simulations [22], should be revisited.

[1] P. Ring and P. Schuck, *The Nuclear Many-Body Problem* (Springer-Verlag, Berlin, 1980).  
 [2] G. F. Bertsch and S. Das Gupta, Phys. Rep. **160**, 4 (1988); R. Malfliet, Prog. Part. Nucl. Phys. **21**, 207 (1988) and references therein.

[3] T. L. Ainsworth *et al.*, Nucl. Phys. **A464**, 740 (1987) and references therein.  
 [4] C. Gale, G. F. Bertsch, and S. Das Gupta, Phys. Rev. C **35**, 1666 (1987).  
 [5] J. Aichelin, A. Rosenhauer, G. Peilert, H. Stoecker, and W.

- Greiner, Phys. Rev. Lett. **58**, 1926 (1987).
- [6] F. Sebille *et al.*, Nucl. Phys. **A501**, 137 (1989).
- [7] D. Gogny, in *Nuclear Self-Consistent Field*, edited by G. Ripka and M. Porneuf (North-Holland, Amsterdam, 1975), p. 333.
- [8] M. Prakash, T. T. S. Kuo, and S. Das Gupta, Phys. Rev. C **37**, 2253 (1988).
- [9] H. Stoecker and W. Greiner, Phys. Rep. **137**, 277 (1986).
- [10] W. Bauer, C. K. Gelbke, and S. Pratt, Annu. Rev. Nucl. Part. Sci. **42**, 77 (1992).
- [11] Ch. Gregoire *et al.*, Nucl. Phys. **A465**, 315 (1987).
- [12] A. Bonasera *et al.*, Phys. Rep. **244**, 1 (1994); A. Bonasera, G. F. Burgio, and M. DiToro, Phys. Lett. B **221**, 233 (1989); A. Bonasera and F. Gulminelli, *ibid.* **259**, 399 (1991).
- [13] R. J. Lenk and V. R. Pandharipande, Phys. Rev. C **39**, 2242 (1989).
- [14] A. Guarnera, computer code TWINGO code, Ph.D. thesis, University of Caen, 1996.
- [15] M. Colonna *et al.*, Nucl. Phys. **A541**, 295 (1992).
- [16] M. Colonna *et al.*, Phys. Lett. B **283**, 180 (1992).
- [17] B. Faure *et al.*, Phys. Rev. C **35**, 190 (1987).
- [18] V. Greco, Master thesis, University of Catania, 1997.
- [19] V. de la Mota *et al.*, Phys. Rev. C **46**, 677 (1992); V. de la Mota *et al.*, Z. Phys. A **343**, 417 (1992).
- [20] M. Colonna, M. DiToro, and A. Guarnera, Nucl. Phys. **A589**, 160 (1995).
- [21] M. F. Rivet *et al.*, Phys. Lett. B **388**, 219 (1996).
- [22] W. Cassing, V. Metag, U. Mosel, and K. Niita, Phys. Rep. **188**, 363 (1990); W. Cassing and U. Mosel, Prog. Part. Nucl. Phys. **25**, 235 (1990).